

Quantifying pulmonary perfusion from noncontrast computed tomography

Edward Castillo^{a)}

Department of Radiation Oncology, Beaumont Health, Royal Oak, MI, USA

Department of Computational and Applied Mathematics, Rice University, Houston, TX, USA

Girish Nair

Department of Internal Medicine, Beaumont Health, Royal Oak, MI, USA

Danielle Turner-Lawrence

Department of Emergency Medicine, Beaumont Health, Royal Oak, MI, USA

Nicholas Myziuk

Department of Radiation Oncology, Beaumont Health, Royal Oak, MI, USA

Scott Emerson and Sayf Al-Katib

Department of Diagnostic Radiology, Beaumont Health, Royal Oak, MI, USA

Sarah Westergaard and Richard Castillo

Department of Radiation Oncology, Emory University, Atlanta, GA, USA

Yevgeniy Vinogradskiy

Department of Radiation Oncology, University of Colorado, Denver, CO, USA

Thomas Quinn, Thomas Guerrero and Craig Stevens

Department of Radiation Oncology, Beaumont Health, Royal Oak, MI, USA

(Received 17 September 2020; revised 14 January 2021; accepted for publication 8 February 2021; published 11 March 2021)

Purpose: Computed tomography (CT)-derived ventilation methods compute respiratory induced volume changes as a surrogate for pulmonary ventilation. Currently, there are no known methods to derive perfusion information from noncontrast CT. We introduce a novel *CT-Perfusion* (CT-P) method for computing the magnitude mass changes apparent on dynamic noncontrast CT as a surrogate for pulmonary perfusion.

Methods: *CT-Perfusion* is based on a mass conservation model which describes the unknown mass change as a linear combination of spatially corresponding inhale and exhale HU estimated voxel densities. CT-P requires a deformable image registration (DIR) between the inhale/exhale lung CT pair, a preprocessing lung volume segmentation, and an estimate for the Jacobian of the DIR transformation. Given this information, the CT-P image, which provides the magnitude mass change for each voxel within the lung volume, is formulated as the solution to a constrained linear least squares problem defined by a series of subregional mean magnitude mass change measurements. Similar to previous robust CT-ventilation methods, the amount of uncertainty in a subregional sample mean measurement is related to measurement resolution and can be characterized with respect to a tolerance parameter τ . Spatial Spearman correlation between single photon emission CT perfusion (SPECT-P) and the proposed CT-P method was assessed in two patient cohorts via a parameter sweep of τ . The first cohort was comprised of 15 patients diagnosed with pulmonary embolism (PE) who had SPECT-P and 4DCT imaging acquired within 24 h of PE diagnosis. The second cohort was comprised of 15 nonsmall cell lung cancer patients who had SPECT-P and 4DCT images acquired prior to radiotherapy. For each test case, CT-P images were computed for 30 different uncertainty parameter values, uniformly sampled from the range [0.01, 0.125], and the Spearman correlation between the SPECT-P and the resulting CT-P images were computed.

Results: The median correlations between CT-P and SPECT-P taken over all 30 test cases ranged between 0.49 and 0.57 across the parameter sweep. For the optimal tolerance $\tau = 0.0385$, the CT-P and SPECT-P correlations across all 30 test cases ranged between 0.02 and 0.82. A one-sample sign test was applied separately to the PE and lung cancer cohorts. A low Spearman correlation of 15% was set as the null median value and two-sided alternative was tested. The PE patients showed a median correlation of 0.57 (IQR = 0.305). One-sample sign test was statistically significant with 96.5% confidence interval: 0.20–0.63, $P < 0.00001$. Lung cancer patients had a median correlation of 0.57 (IQR = 0.230). Again, a one-sample sign test for median was statistically significant with 96.5% percent confidence interval: 0.45–0.71, $P < 0.00001$.

Conclusion: *CT-Perfusion* is the first mechanistic model designed to quantify magnitude blood mass changes on noncontrast dynamic CT as a surrogate for pulmonary perfusion. While the reported

correlations with SPECT-P are promising, further investigation is required to determine the optimal CT acquisition protocol and numerical method implementation for CT-P imaging. © 2021 The Authors. *Medical Physics* published by Wiley Periodicals LLC on behalf of American Association of Physicists in Medicine. [https://doi.org/10.1002/mp.14792]

Key words: 4DCT, computed tomography, deformable image registration, perfusion, SPECT perfusion, ventilation

1. INTRODUCTION

Computed tomography (CT)-derived ventilation (CT-V) is an image processing modality that quantifies voxel volume changes within an inhale/exhale CT image pair as a surrogate for pulmonary ventilation.^{1,2} CT-V has become increasingly utilized in radiation oncology for functional avoidance radiotherapy.^{3,4} In particular, CT-V has been used for functional avoidance radiotherapy where the radiation plan is designed to avoid functional portions of the lungs as measured by CT-V.⁵ The major advantage of CT-V in the radiation oncology domain is that patients routinely undergo four-dimensional CT (4DCT) as part of standard of care prior to radiation therapy; therefore, functional CT-V information can be obtained without the need for extra imaging procedures. While preliminary results for CT-V functional avoidance have been positive,³ a complete picture of lung function includes ventilation (airflow) and perfusion (blood flow). Thus, methods for computing perfusion information from noncontrast inhale/exhale CT image pairs could potentially improve CT-V functional avoidance strategies. However, there are no current methods for quantifying perfusion from noncontrast CT.

Clinical utility of a noncontrast-based measure of pulmonary perfusion is not limited to the field of radiation oncology. Pulmonary embolism (PE) is associated with a high short-term mortality, but is often difficult to diagnose on presentation.⁶ While CT pulmonary angiography (CTA) is the gold standard for accurate and rapid diagnosis of PE, there are limited diagnostic options for those who cannot undergo CTA due to contrast allergy or renal disease. Moreover, technical challenges of CTA, including respiratory motion artifact and suboptimal intravenous contrast bolus, can lead to nondiagnostic exams in up to 43% in some patient populations.⁷ Single photon emission computed tomography (SPECT) ventilation-perfusion imaging has been shown to be effective,^{8,9} but is time-consuming to acquire and, unlike CT, is not readily available in most emergency centers. Coupled with CT-V, perfusion imaging derived from noncontrast CT could be an additional diagnostic tool in certain situations for the diagnosis of PE. Motivated by the goal of potentially impacting clinical applications, such as radiotherapy functional avoidance planning and pulmonary embolism diagnostics, in this work, we propose a novel mechanistic physical model for generating noncontrast CT-based perfusion images.

There are two primary classes of CT-V algorithms, intensity-based and transformation-based. CT-V methods require image segmentation to delineate the lung volume and deformable image registration (DIR) to provide a spatial

transformation between the inhale and exhale lung geometries. As opposed to transformation-based methods, which recover volume changes directly from the Jacobian factor of the DIR solution,^{10,11} intensity or Hounsfield Unit (HU) methods estimate volume changes from the variations between the HU values of spatially corresponding inhale/exhale voxels.^{1,12} HU represents material density on a linear scale where -1000 HU corresponds to air and 0 HU water (or tissue). Intensity-based ventilation methods are mathematically built on the assumption that lung tissue can be physically modeled as a linear combination of air and tissue components, an approach first proposed by Simon in the context of computing specific lung compliance.¹³ A consequence of the air/tissue model is that material density within the lungs can be approximated (in units: g/ml) as Ref. [1,14]:

$$\rho(\mathbf{x}) = 1 + \frac{HU(\mathbf{x})}{1000}. \quad (1)$$

Most CT ventilation methods operate under the assumption that HU and, consequently, density variations within inhale/exhale CT images are caused solely by changes in air content. This assumption implies that mass is constant within the lung volume throughout the entire breath cycle.¹² However, pulmonary capillary blood volume and gas exchange from the alveoli to capillary side increases proportionately with lung volume¹⁵ and there is a cyclical variation in blood volume within the lung at any time point of the respiratory cycle, increasing with inspiration during normal breathing.^{16–18} Thus, mass change within the lung volume during the respiratory cycle reflects changes in pulmonary blood volume. Moreover, previous studies have shown that there is an observable difference in lung tissue mass between inhale and exhale segmented lung volumes based on Eq. (1),^{14,19} indicating that pulmonary blood mass dynamics can be quantified from noncontrast inhale/exhale CT image pairs.

Recognizing that blood mass variations within the lung during respiration are a fundamental violation of the constant lung mass assumption employed by most CT-ventilation algorithms,¹² a global scaling factor, which assumes a uniform perfusion effect, is often applied as a correction to simulate mass consistency between segmented lung volumes.^{2,20} It is also possible to derive a modification of Simon's model that accounts for the mass change variations by incorporating the Jacobian factor computed from the DIR transformation.²¹ Though the approach is not designed to estimate perfusion, the resulting "hybrid" ventilation methods seemingly correct for the shortcomings associated with the purely HU-based mass conserving approach. However,

standard finite difference-based approximations for the DIR Jacobian factor have been shown to be numerically unstable, whereby small magnitude perturbations to the DIR displacement field (on the order of a single voxel) can result in significant changes in the Jacobian-estimated volume change.²² This, in part, contributes to the issues regarding low-reproducibility of CT-ventilation previously reported in the literature,^{23–26} and introduces numerical instability into Jacobian-based mass correction approaches. Having identified the numerical challenges associated with Jacobian volume change estimation, we previously developed a new class of robust CT-ventilation algorithms designed to address them^{11,12} and demonstrated that the robust algorithms have a higher spatial correlation with single photon emission computed tomography (SPECT) ventilation than any previously reported methods.²⁷

While previous studies have examined total lung and gross regional mass variations,¹⁹ there are currently no methods for computing voxel level magnitude blood mass changes from dynamic noncontrast CT. *The purpose of this study is to (a) introduce the CT-Derived Perfusion (CT-P) imaging method for computing magnitude blood mass changes that occur between an inhale/exhale CT image pair as a surrogate for pulmonary perfusion, and (b) characterize the spatial correlation between CT-perfusion and SPECT perfusion (SPECT-P) imaging.* CT-P employs physical modeling and numerical optimization to recover magnitude blood mass change at the voxel level, which results in a CT-derived perfusion image. The proposed CT-P method builds upon our previous work on robust HU-based CT ventilation and follows a similar numerical implementation.¹¹ As such, the CT-P algorithm is based on first computing a series of magnitude mass change measurements between spatially corresponding inhale/exhale lung subregions. The uncertainty in the subregional measurements is modeled with Gaussian statistics. This allows the uncertainty to be controlled through the definition of an uncertainty tolerance parameter. While this approach provides robustness to DIR variability, it does so at the expense of measurement resolution. We characterize the spatial correlation between CT-P and SPECT-P using a systematic sweep of the tolerance parameter and imaging data from two patient cohorts. The first cohort is comprised of patients treated with radiotherapy for nonsmall cell lung cancer and the second is comprised of patients diagnosed with pulmonary embolism.

2. MATERIALS AND METHODS

2.A. CT-derived perfusion formulation

Equation (1) converts an inhale/exhale CT image pair into two corresponding density functions which we denote as the reference image $R(\mathbf{x})$, and the target image $T(\mathbf{x})$. The distinction is irrelevant (i.e., inhale and exhale can correspond to reference and target or vice versa). A spatial transformation

$\phi: \mathbb{R}^3 \rightarrow \mathbb{R}^3$ computed with a DIR algorithm maps the reference image lung volume $\Omega^{(R)}$ onto the target image lung volume $\Omega^{(T)}$:

$$\Omega^{(T)} = \phi\left(\Omega^{(R)}\right). \quad (2)$$

Unlike previous CT-ventilation formulations,¹² for a general subregion $\Omega \in \Omega^{(R)}$, our proposed CT-perfusion formulation allows mass to fluctuate in order to explicitly account for any potential blood mass variations:

$$\int_{\Omega} R(\mathbf{x}) d\mathbf{x} - \int_{\Omega} \hat{P}(\mathbf{x}) d\mathbf{x} = \int_{\phi(\Omega)} T(\mathbf{x}) d\mathbf{x} = \int_{\Omega} T(\phi(\mathbf{x})) J(\mathbf{x}) d\mathbf{x}, \quad (3)$$

where $\int \hat{P}(\mathbf{x}) d\mathbf{x}$ represents the signed total difference in mass between the reference volume $\Omega \in \Omega^{(R)}$ and the target volume $\phi(\Omega) \in \Omega^{(T)}$, and J is the Jacobian factor of ϕ . The Jacobian factor itself is a well-known surrogate for pulmonary ventilation and can be estimated robustly using the transformation-based Integrated Jacobian Formulation (IJF) method.¹¹ Thus, the magnitude blood mass difference estimation for Ω is defined as:

$$\int_{\Omega} P(\mathbf{x}) d\mathbf{x} = \int_{\Omega} |R(\mathbf{x}) - T(\phi(\mathbf{x})) J(\mathbf{x})| d\mathbf{x}, \quad (4)$$

where the integrand on the right side of the equation is a data term defined entirely from measurable quantities, namely, the reference image, target image, DIR transformation, and Jacobian. Our proposed CT-P imaging recovers the unknown P using the Eq. (4) formulation.

We point out that making the standard CT-V mass consistency assumption implies $\hat{P} = 0$. From Eq. (3), this assumption allows the Jacobian factor to be described strictly in terms of the HU-estimated density values. A robust HU-based CT-V strategy for recovering the Jacobian factor from Eq. (3), under the assumption that $\hat{P} = 0$, has previously been described.¹²

2.B. Estimating subregional magnitude mass change

Since the right side of Eq. (4) is comprised of measurable quantities, a straightforward implementation would be to simply let Ω be a single voxel volume centered on grid location \mathbf{x} and set $P(\mathbf{x}) = |R(\mathbf{x}) - T(\phi(\mathbf{x})) J(\mathbf{x})|$. However, similar to the situation that arises in HU-based ventilation methods,¹² this naïve approach is susceptible to corruption from image noise, errors in the DIR mapping, and errors in the Jacobian estimation. As demonstrated in Refs. [11,12], statistical modeling can be used to both describe the uncertainties associated with potential errors and provide some guidance on how to control them.

Standard Monte Carlo integration methods, under mild assumptions, express an integral in terms of the integrand average over a desired volume.²⁸ Applying this approach to Eq. (4) yields:

$$\int_{\Omega} P(\mathbf{x}) d\mathbf{x} = \bar{P}_{\Omega} \cdot \text{vol}(\Omega) \approx \left(\frac{1}{|\Omega|} \sum_{\mathbf{x}_i \in \Omega} |R(\mathbf{x}_i) - T(\phi(\mathbf{x}_i))J(\mathbf{x}_i)| \right) \cdot \text{vol}(\Omega) = \langle P \rangle_{\Omega} \cdot |\Omega|,$$

where the integrand sample mean, $\langle P \rangle_{\Omega}$, can be computed directly from known image data. Assuming Gaussian statistics on Ω , the uncertainty in the sample mean, $\langle P \rangle_{\Omega}$, is characterized by the corresponding standard error. However, image data are provided only on the voxel locations. As previously described in Ref. [12], there is a tradeoff between sample mean fidelity and measurement resolution. Larger $M = |\Omega|$ reduces the uncertainty in the sample mean estimate, but requires the measurement be taken over a larger subregional volume. Since the Eq. (1) HU-estimated density values are less than or equal to one, we assume $0 \leq P(\mathbf{x}) \lesssim 1$. As described in Ref. [12], this implies that given a specified tolerance τ and scalar constant $\beta = 1.96$

$$|\bar{P}_{\Omega} - \langle P \rangle_{\Omega}| \leq \tau, \quad (6)$$

with greater than 95% probability when Ω is chosen such that

$$M \geq \frac{\beta^2}{\tau^2}. \quad (7)$$

2.C. CT-perfusion image generation

A full CT-P image, $P(\mathbf{x})$, requires computing the discretized variables

$$p_i = P(\mathbf{x}_i), \quad \forall \mathbf{x}_i \in \Omega^{(R)}, \quad (8)$$

where $p_i > 0$ represents the magnitude mass change of the undeformed unit volume voxel centered on \mathbf{x}_i . Our proposed numerical method follows the framework used for our previously described robust CT-ventilation methods,^{11,12} and is based on approximating the Eq. (5) integral for a series of subvolumes $\Omega_k \in \Omega^{(R)}$, $k = 1, 2, \dots, K$. For $|\Omega^{(R)}| = N$, the subvolume data acquisition process results in a linear system of equations describing the unknown p_i :

$$\begin{aligned} Ap &= b, \\ A \in \mathbb{R}^{K \times N}, \quad b \in \mathbb{R}^{K \times 1}, \quad p \in \mathbb{R}^{N \times 1}, \end{aligned} \quad (9)$$

where

$$A_{ki} = \begin{cases} \frac{1}{|\Omega_k|} & \text{if } \mathbf{x}_i \in \Omega_k \\ 0 & \text{otherwise} \end{cases}, \quad (10)$$

and the elements of b contain the corresponding subregional sample mean estimates $\langle P \rangle_{\Omega_k}$ [Eq. (5)]. Depending on image resolution, the number of unknowns, N , can be large (on the order of 10^8). Thus, in order to lower overall computational complexity and memory storage requirements, we parameterize $P(\mathbf{x})$ using moving least squares.

Given a set of L knot locations $\mathbf{z}_j \in \Omega^{(R)}$ with corresponding scalar parameter values q_j , the Shepard's class of moving

least squares approximation is defined as:

$$P(\mathbf{x}_i; q) = p_i = \frac{\sum_{j=1}^L w(\|\mathbf{x}_i - \mathbf{z}_j\|) (q_j)}{\sum_{j=1}^L w(\|\mathbf{x}_i - \mathbf{z}_j\|)}, \quad (11)$$

where the proximal weighting function is of the form

$$w(r) = e^{-\sigma r^2}. \quad (12)$$

The Eq. (12) parameterization reduces the number of unknowns required to generate the magnitude mass change (perfusion) image from N (the total number of voxels in the reference lung region of interest) down to L (the number of knots used for the discretization). The image is recovered by solving the following constrained linear least squares problem:

$$\begin{aligned} \min_q \quad & \|\hat{A}q - b\|^2 \\ \text{s.t.} \quad & \\ & q_i \geq 0, \quad i = 1, 2, \dots, L, \end{aligned} \quad (13)$$

where

$$\begin{aligned} \hat{A} &= AC, \\ \hat{A} &\in \mathbb{R}^{K \times L}, \quad C \in \mathbb{R}^{N \times L}, \end{aligned} \quad (14)$$

and

$$C_{ij} = \frac{w(\|\mathbf{x}_i - \mathbf{z}_j\|)}{\sum_{l=1}^L w(\|\mathbf{x}_i - \mathbf{z}_l\|)}. \quad (15)$$

Choosing the number of subregional measurements such that $N \geq K \gg L$ results in an over-determined system of equations, while the Eq. (13) inequality constraints corresponds to the fact that $P(\mathbf{x}; q)$ represents magnitude mass change. The solution to Problem (13), $P(\mathbf{x}; q)$, represents a density function in the same g/ml units as Eq. (1). Magnitude mass change for the voxel volume v_i centered on \mathbf{x}_i , as defined by Eq. (4), can therefore be computed as:

$$P(\mathbf{x}_i, q) \cdot \text{vol}(v_i) \approx \bar{P}_{v_i} \cdot \text{vol}(v_i) = \int_{v_i} P(\mathbf{x}; q) d\mathbf{x}. \quad (16)$$

Voxel volume is constant on the image grid but is an acquisition parameter that can vary from image-to-image. Thus, we simply take $P(\mathbf{x}; q)$ as our perfusion surrogate.

2.D. Numerical implementation

All softwares were written in MATLAB release R2019a (The Mathworks Inc, Natick, Massachusetts, United States). The maximum inhale and exhale 4DCT phases were used for the study. Lung masks were generated using a semi-automated histogram segmentation (as done in Ref. [2]). A dart-throwing algorithm²⁹ was applied to $\Omega^{(R)}$ in order to generate MLS knot locations, $\mathbf{z}_j \in \Omega^{(R)}$, with approximately 30-mm

uniform spacing. Similar to the number of cubic spline knots used for lung CT DIR,³⁰ this procedure results in approximately 250–300 knots. An additional point cloud is similarly acquired with approximately 7-mm uniform spacing to serve as the subdomain locations for Eq. (9). This results in approximately 20 000 to 30 000 subdomain measurement points. Each initial Ω_k subdomain was defined as a single voxel and then morphologically dilated with a $7 \times 7 \times 3$ voxel structuring element until the desired Eq. (7) tolerance criteria was satisfied. In addition, the MATLAB soutlance function was applied to provide further robustness to any potential DIR inaccuracies when computing $\langle P \rangle_{\Omega_k}$. Equation (13) is solved using the interior point method implemented in the MATLAB optimization routine lsqin. For all experiments, CT-P is computed on the exhale phase. Thus for Eq. (4), the exhale phase is the reference image and inhale phase is the target image.

2.E. DIR and Jacobian estimation

The sample mean estimates defined by Eq. (5) require both the DIR transformation ϕ and the volume change it induces, which is given by J (the Jacobian factor of ϕ). The Jacobian factor is computed using the parameterized Integrated Jacobian Formulation (IJF) method described in Ref. [27], which determined that the uncertainty parameter $\tau_{IJF} = 0.07$ generates an optimal spatial correlation between SPECT-ventilation and 4DCT-derived ventilation.

The Quadratic Penalty DIR (QPDIR) algorithm was used to compute to ϕ for the CT-P method and ϕ^{-1} for the IJF method (see Refs. [11,27] for more details on IJF). Briefly, QPDIR is an intensity-based algorithm designed around a gradient-free block coordinate descent strategy that iterates between block matching operations and linear least squares solves to minimize the structural similarity index between an image pair. The implementation follows the description in Ref. [31], with the exception that an additional sum-of-squared difference term was included in the QPDIR objective function to ensure lung mask alignment (as done in Ref. [32]).

2.F. Image data

Analysis of the proposed CT-P method was conducted using the 4DCT and Single Photon Emission Computed Tomography perfusion (SPECT-P) images from two patient cohorts. The first cohort is comprised of 15 patients with pulmonary embolism treated at our institution. Data were acquired as part of a prospective imaging trial and evaluated according to an IRB approved study (IRB 2017-018, clinicaltrials.gov #NCT03183063). Patients diagnosed with pulmonary emboli on CTA were recruited to the study. The 4DCT and SPECT-P images were acquired within 48 h of the PE diagnosis in order to ensure any clinical lung function changes occurring due to treatment would be minimal.

The second patient cohort is comprised of 15 NSCLC patients who received radiotherapy at our institution. Data were retrospectively evaluated according to an IRB approved study (IRB 2016-037, clinicalTrials.gov #NCT02528942). Patients received definitive radiotherapy (defined as prescription doses of 45 to 75 Gy) and a planned concurrent chemotherapy regimen. The majority of enrolled patients had stage III disease. SPECT-P imaging was acquired prior to delivery of the first radiotherapy fraction, ensuring no clinical lung function changes occurred due to treatment between the simulation 4DCT and SPECT-P acquisitions.

2.F.1. Pulmonary embolism Cohort 4DCT acquisition

Four-dimensional CT images were acquired in supine position on a General Electric Revolution Evo 64-slice scanner operating in sequential cine mode. Patients with BMI < 30 were scanned with 100 kVp, 27.5 mAs, and a CTDI 32.7 mGy. Patients with BMI > 30 were scanned with 120 kVp, 17.5 mAs, and a CTDI 33.6 mGy. Both patient groups shared the common 40 mm beam collimator (64×0.625 mm configuration), 500 ms tube rotation speed, 22 consecutive acquisitions per beam width, digitally reconstructed to 16 slices with a 2.5-mm slice thickness, 2.5-mm slice increment, and with a 7.5-mm overlap to the previous beam setting. Patients were coached by support staff to maintain a constant breathing rate, prior to imaging. Images were reconstructed trans-axially (512×512 pixels per 2D slice image, voxel dimensions of $0.97 \text{ mm} \times 0.97 \text{ mm} \times 2.5 \text{ mm}$) and exported into DICOM format. The full inhale and exhale phases were reconstructed from the cine images using a quantitative image correlation-based sorting method.³³

2.F.2. Lung cancer cohort 4DCT acquisition

A Philips Brilliance Big Bore CT (version 3.6.7) with a bellows system was used for respiratory correlated imaging. The 4DCT images were acquired with x-ray tube settings of 120 kVp and 599 mAs, and reconstructed using phase binning to produce an average CT image and 10 phase indexed CT images. The phase images were indexed from 0% to 90% in steps of 10% where 0% indicates full inhalation and 50% indicates full exhalation on the breathing curve. Final images were then exported into the DICOM standard (512×512 pixels per 2D slice image, voxel dimensions of $1.27 \text{ mm} \times 1.27 \text{ mm} \times 3 \text{ mm}$).

2.F.3. SPECT perfusion acquisition

SPECT-P images were acquired on a dual head Siemens Symbia SPECT/CT scanner (Siemens Medical Solutions, USA), using a parallel hole, high-resolution collimator and an energy window of 15% at a centerline of 140 keV. Perfusion ($^{99\text{m}}\text{Tc}$ -MAA SPECT/CT) imaging was conducted following IV administration of 4.0 mCi of $^{99\text{m}}\text{Tc}$ -MAA

(Lantheus Medical Imaging, Billerica, MA) with the patient lying supine during tidal respiration. Ventilation imaging was not acquired for the PE cohort. SPECT acquisition was performed in steps of 6° for the entire 360° of rotation, with a 25 s collection time for each step. Total scan acquisition time for most patients was under 30 min. Free breathing, attenuation corrected CT images were subsequently recorded with 130 kVp, and 75–100 mAs (weight dependent) during continuous tidal respiration. The final reconstructed SPECT images were then exported into DICOM (64 x 64 pixel per 2D slice image, voxel dimensions 6.00 mm x 6.00 mm x 2.00 mm).

2.G. CT-perfusion and SPECT perfusion spatial correlation assessment

A parameter sweep was conducted in order to assess the effect of the uncertainty tolerance τ on the spatial correlation between SPECT-P and the resulting CT-P images. For each of the 30 test cases (15 from each of the two patient cohorts), a series of 30 CT-P images were computed using a uniformly sampled set of uncertainty tolerances ranging between $\tau \in [0.01, 0.125]$. Each resulting CT-P image was spatially aligned with the SPECT-P image by first using affine registration to align the exhale 4DCT phase (on which the CT-P is computed) and the SPECT attenuation correction CT. The resulting affine transformation was then applied to the CT-P

image and the voxel-wise Spearman correlation was computed at the resolution of the SPECT-P after applying a median filter with 3×3 structuring element to the SPECT image (as done in Ref. [34]).

3. RESULTS

The median Spearman correlations between SPECT-P and CT-P taken across all 30 test cases for each uncertainty parameter value included in the sweep are presented in Fig. 1. The median correlation values were relatively consistent across the parameter sweep, ranging between 0.49 and 0.57 with the highest values being achieved for $\tau \in [0.0285, 0.0385]$. The median correlation within each cohort are plotted separately in Fig. 2.

As summarized in Table I, for an optimal $\tau = 0.0385$ (chosen within the optimal range $\tau \in [0.0285, 0.0385]$) the CT-P and SPECT-P Spearman correlations across the 15 test cases in the PE cohort ranged between 0.02 and 0.77. Similarly, across the 15 cases in the lung cancer cohort, the correlations ranged between 0.10 and 0.82. A Shapiro–Wilk normality test was significant for PE indicating data skewness. As such, all comparisons were conducted with respect to median values.

A one-sample sign test was applied separately to the PE and lung cancer cohorts. A low Spearman correlation of 0.15 was set as the null median value in order account for any possible inherent correlation between CT-P and SPECT-P

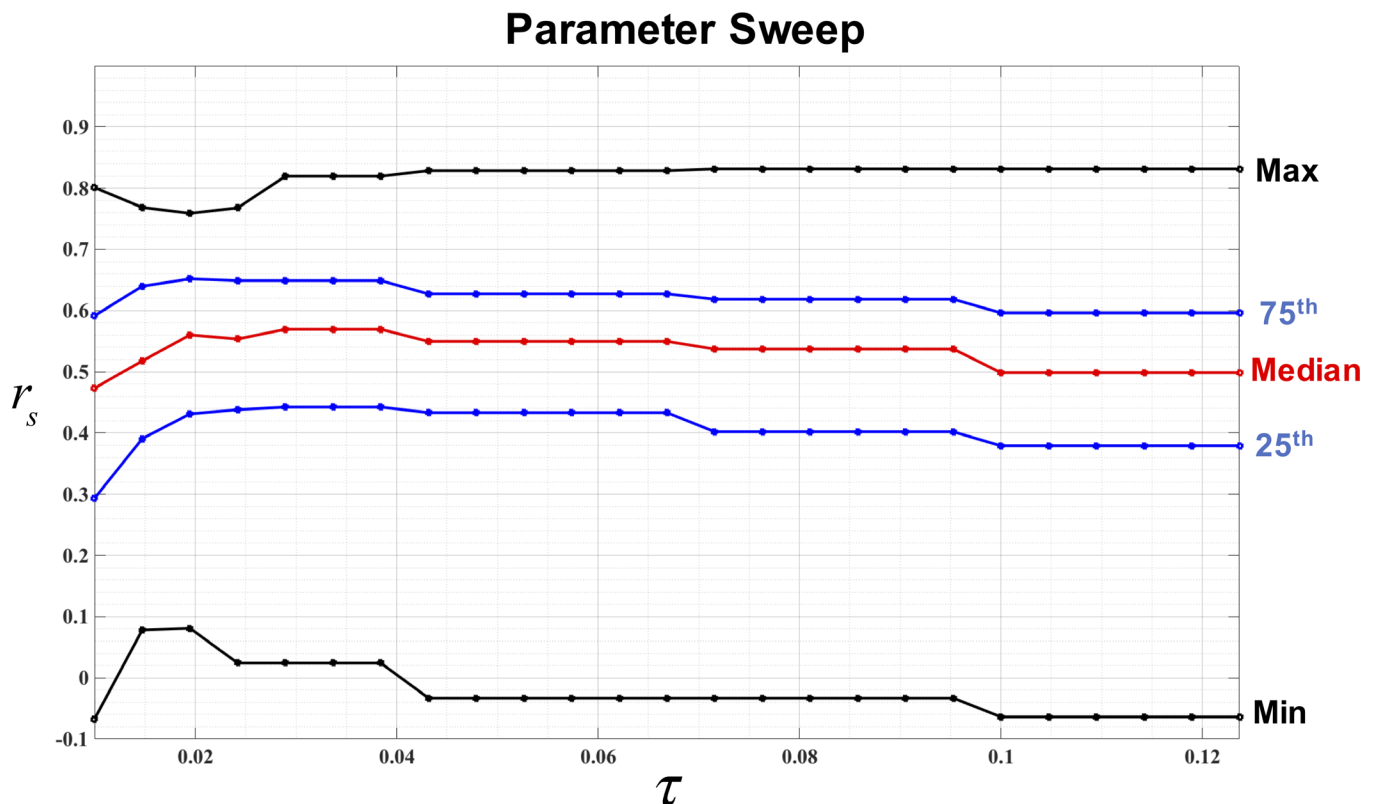


FIG. 1. The maximum, 75th percentile, median, 25th percentile, and minimum CT-P and SPECT-P Spearman correlations, r_s , across all 30 test cases (PE and Lung Cancer cohorts combined) as a function of the uncertainty parameter τ are plotted. The median correlation values remain relatively constant across the parameter sweep. [Color figure can be viewed at wileyonlinelibrary.com]

Parameter Sweep (Cohorts)

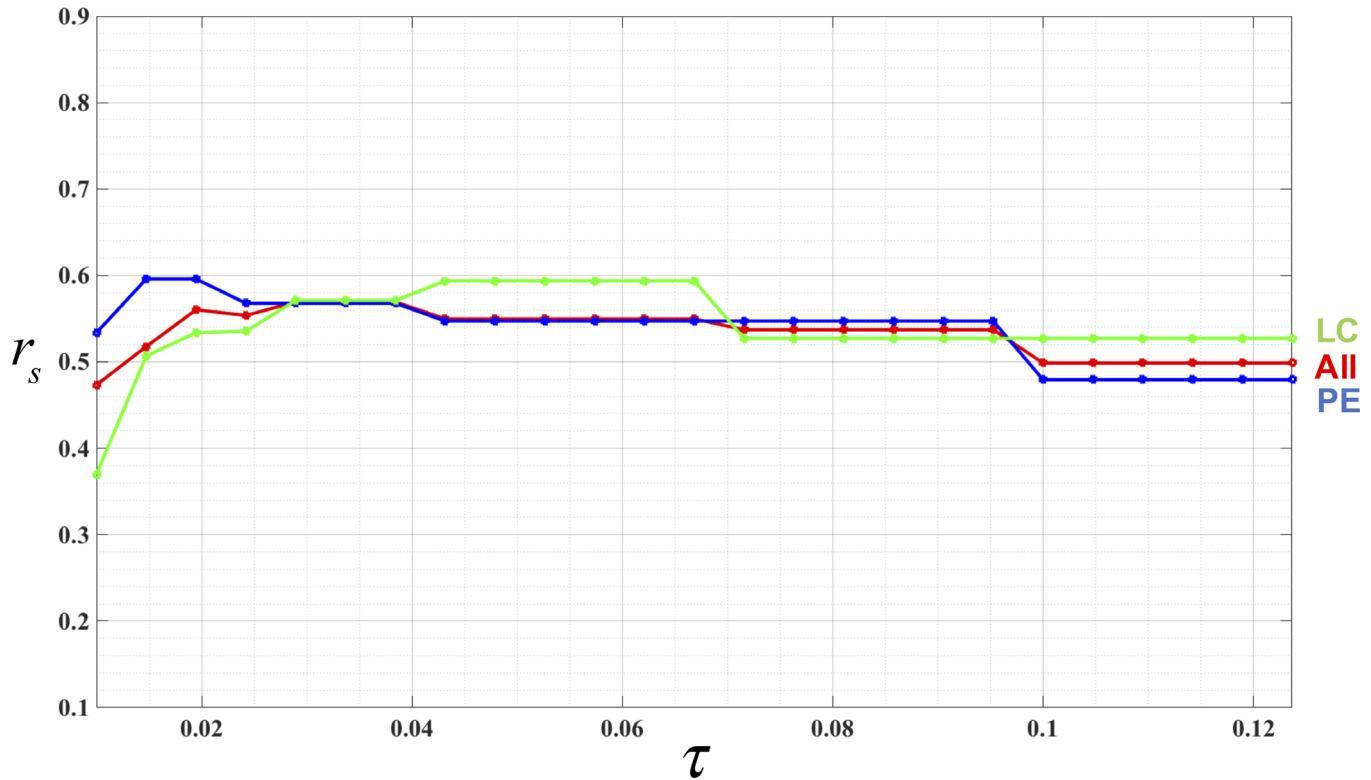


FIG. 2. The median CT-P and SPECT-P Spearman correlations, r_s , across the 15 patients in the PE cohort (PE, blue) and Lung Cancer cohort (LC, green) as a function of the uncertainty parameter τ are plotted. The median across all 30 test cases (PE and Lung Cancer cohorts combined) is also provided (All, red). The median correlation curve for each cohort shows that for smaller τ (high certainty, low resolution) correlation with SPECT-P is lower, indicating insufficient resolution in the subregional measurements to accurately describe spatial variations in pulmonary function. A similar, though not as pronounced, drop in correlation is also seen for $\tau > 0.095$ (low certainty, higher resolution), indicating the effects of uncertainty and more erroneous subregional mass change measurements.

TABLE I. CT-perfusion and SPECT-P Spearman correlations for optimal $\tau = 0.385$.

Case #	Pulmonary embolism cohort	Lung cancer cohort
1	0.55	0.10
2	0.61	0.57
3	0.65	0.65
4	0.02	0.72
5	0.70	0.50
6	0.44	0.45
7	0.57	0.73
8	0.62	0.82
9	0.51	0.53
10	0.17	0.71
11	0.11	0.70
12	0.20	0.43
13	0.63	0.50
14	0.61	0.37
15	0.77	0.61
Median	0.57	0.57

The Spearman correlations between SPECT-Perfusion and CT-Perfusion (CT-P) for the pulmonary embolism patient cohort and lung cancer cohort, using the optimal uncertainty tolerance $\tau = 0.385$. Wilcoxon signed-rank test applied to the correlations from the two cohorts reveals no significant difference, indicating that the CT-P method’s performance is consistent between the two patient cohorts.

stemming from the fact that the images were acquired for the same patient. A two-sided alternative was tested. The PE patients showed a median correlation of 0.57 (IQR = 0.305). The one-sample sign test was statistically significant with 96.5% confidence interval: 0.20–0.63, $P < 0.00001$. Lung cancer patients had a median correlation of 0.57 (IQR = 0.230). Again, the one-sample sign test for median was statistically significant with 96.5% confidence interval: 0.45–0.71, $P < 0.00001$. Moreover, a two-sided Wilcoxon signed-rank test indicated that the difference between the median correlations observed in the two cohorts was not significant ($P = 0.49$). Figure 3 illustrates the CT-P and SPECT-P images for representative PE case 5 and Fig. 4 illustrates the images for representative Lung Cancer case 8.

4. DISCUSSION

In previous work, we described a robust HU-based CT-ventilation approach, referred to as the Mass Conserving Volume Change (MCVC) estimation method,¹² which was premised on the assumption that mass within the lung volume remains constant throughout the breath-cycle. This assumption, which implies that any HU variations are caused strictly by changes in air content, is in fact the foundation of all HU-based CT-ventilation methods.² However, the

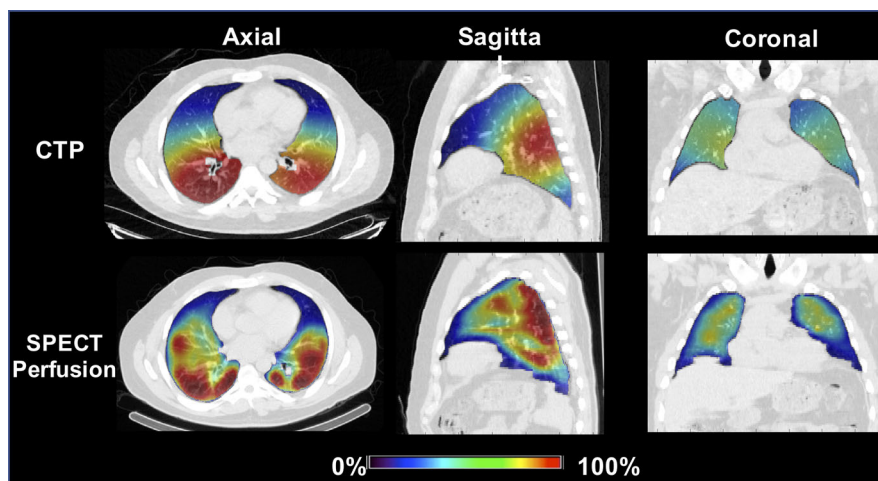


FIG. 3. Axial (Left), sagittal (middle), and coronal (right) slices from the CT-Perfusion (CTP) (top row) and SPECT Perfusion (bottom row) images for test case 5 in the PE cohort (Table I). The Spearman correlation between the spatially aligned CTP and SPECT-Perfusion values is 0.70. For visualization, the intensity values within each image were converted to percentile values (color scale). Visually, there is good correlation between CT-P and SPECT-P.

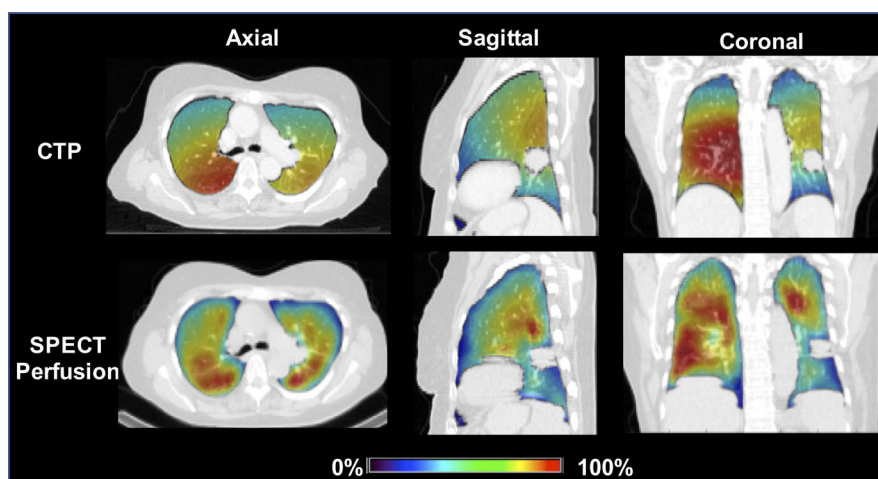


FIG. 4. Axial (Left), sagittal (middle), and coronal (right) slices from the CT-Perfusion (CTP) (top row) and SPECT Perfusion (bottom row) images for test case 11 in the Lung Cancer cohort (Table I). The Spearman correlation between the spatially aligned CTP and SPECT-Perfusion values is 0.70. For visualization, the intensity values within each image were converted to percentile values (color scale). Both CTP and SPECT-P show decreased perfusion in the patient's left lower lobe.

assumption is known to be invalid due to variations in the spatial distribution of blood mass that occur within the lungs during breathing.¹⁹ In this study, we introduce the novel CT-Perfusion numerical method for quantifying these blood mass variations as a surrogate for pulmonary perfusion. The CT-P formulation builds upon the MCVF formulation and recovers magnitude mass change at the voxel resolution using HU-defined material density estimates and the DIR spatial mapping between the inhale and exhale geometries. Analyzing mapped CT HU values is certainly not a novel concept, beginning with the initial idea for estimating lung compliance¹³ and including, for example, quantitative methods for identifying disease with parametric response mapping.³⁵ However, the CT-Perfusion derivation is the first theoretical treatment that explicitly defines the relationship between mapped HU values and pulmonary function in terms of ventilation and

perfusion surrogates, namely, magnitude mass change and volume change. In fact, the presented Eq. (4) CT-P formulation is defined with respect to the Jacobian of the DIR transformation which itself is a widely accepted surrogate for ventilation.¹⁰

Recently, we demonstrated that voxel volume changes computed with the robust Integrated Jacobian Formulation (IJF) method generate CT-ventilation images that have high spatial correlation with SPECT-ventilation (15 cases, median Spearman correlation 0.82).²⁷ Given recovered IJF volume changes, the numerical implementation of CT-P is based on making a series of subregional magnitude mass change estimates [Eq. (5)]. Similar to robust CT-ventilation methods, uncertainties introduced by DIR errors and image noise into the subregional measurements are characterized with an uncertainty tolerance parameter τ . As described in Eq. (7),

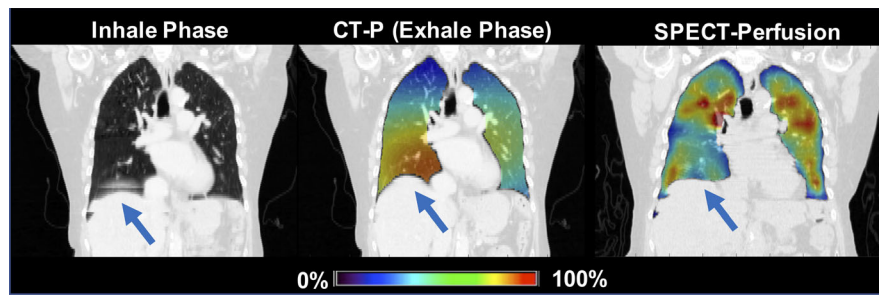


FIG. 5. Corresponding coronal slices from the 4DCT maximum inhale phase (left), CT-Perfusion image superimposed on the maximum exhale phase (middle), and the SPECT-perfusion (right) images for case 1 in the lung cancer cohort from Table I. For visualization, the intensity values within each image were converted to percentile values (color scale). The inhale image possesses a phase-bin artifact (blue arrow), which erroneously elevates the estimated magnitude mass change.

the parameter reflects the fact that robustness is gained at the expense of measurement resolution. Therefore, we characterize the spatial correlation between novel CT-P and SPECT-P using a systematic parameter sweep of τ and imaging data from two patient cohorts (lung cancer and pulmonary embolism) each with 15 patients.

As illustrated by Fig. 1, the median correlation across all 30 test cases was relatively consistent throughout the parameter sweep $\tau \in [0.010 \ 0.125]$, with the highest median value of 0.57 being achieved for $\tau \in [0.0290 \ 0.0385]$. However, for $\tau < 0.015$, which corresponds to low resolution and low uncertainty Eq. (5) subregional measurements, there is a drop off in median correlation. This implies that the low measurement resolution was insufficient for detecting spatial variations in pulmonary perfusion present in the test cases. This effect is more pronounced in the lung cancer cohort than in the PE cohort, as illustrated in Fig. 2, and is consistent with the robust measurement framework. Specifically, the millimeter voxel resolution of the 4DCT imaging acquired for the lung cancer cohort (1.25 mm) is less than that of the 4DCTs acquired for the PE cohort (0.97 mm). The Eq. (6) uncertainty estimate is defined with respect to voxels, not millimeter resolution. As such, a fixed τ corresponds to the number of individual voxel measurements needed to satisfy Eq. (7). This set number of voxels will correspond to a higher resolution in physical space when applied to a CT image with high millimeter resolution, and a lower resolution in physical space when applied to a lower millimeter resolution CT. Thus, the smaller τ values have a larger impact on the lung cohort correlations than on the PE cohort.

Despite the fact that the 4DCTs were acquired with different scanners and different reconstruction parameters, the CT-P and SPECT-P Spearman correlations were relatively consistent between the PE and lung cancer cohorts. Table I details the case-by-case correlations in each cohort for an optimal uncertainty tolerance $\tau = 0.0385$. The median Spearman correlation within each cohort was 0.57 and Wilcoxon rank sum test indicated no statistical difference between them. Moreover, one-sample sign test indicated that the median correlation within each cohort was significantly higher than the null assumption (a low 0.15 correlation). Considering that CT-P is the first method for estimating magnitude mass change as a

surrogate for perfusion, the presented results represent an initial benchmark for this novel class of methods. While direct comparisons are limited, the 0.57 median Spearman correlation between CT-P and SPECT-P compares favorably with previous CT-ventilation validations studies, such as the Ventilation and Medical Pulmonary Image Registration Evaluation (VAMPIRE) study, where the highest performing CT-ventilation methods achieved a median correlation of 0.49 with nuclear medicine imaging.³⁴

The techniques first introduced for robust CT-ventilation and employed within the CT-P numerical method are designed to mitigate the effects of image noise and small errors in the DIR solution.^{11,12} However, these techniques do not account for gross acquisition errors, such as the phase binning artifacts common to 4DCT.²⁴ Artifacts corrupt the geometric and intensity value information needed to estimate both mass change and volume change, thereby reducing overall CT-P efficacy. For example, Fig. 5 shows that case 1 of the lung cancer cohort possesses a phase bin artifact. The artifact causes erroneous high-density diaphragm data to be mapped onto low-density lung parenchyma, which in turn causes an erroneous high magnitude mass change signal in the resulting CT-P image and a lower 0.10 Spearman correlation with the corresponding SPECT-P image. Therefore, breathhold CT acquisitions which avoid binning artifacts may yield more consistent CT-P imaging. Moreover, as described earlier, high-resolution breathhold acquisitions would allow for higher spatial resolution in the subregional measurements acquired for the CT-P numerical method that could translate into higher fidelity imaging. Characterizing the effect of breathhold acquisitions on CT-P performance warrants further study and is an area of our future research.

Taken together with IJF-ventilation, which was previously shown to have high correlation with SPECT-ventilation in lung cancer patients,²⁷ the 0.57 median correlation between CT-P and SPECT-P suggest that CT-P and CT-ventilation have potential utility as diagnostic tools. For instance, while the impacts of PE on lung function are complex, in general, PE results in lung regions with reduced blood flow and preserved ventilation.^{9,36} Figure 6 illustrates a “wedge” perfusion artifact that is common in PE patients.³⁷ Though the wedge is apparent on both the SPECT-P and CT-P images,

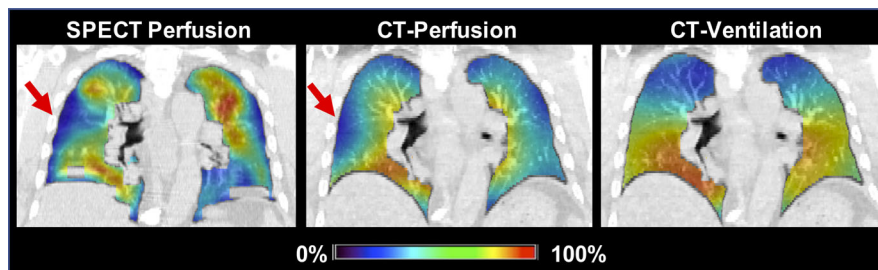


FIG. 6. Coronal images from the SPECT-Perfusion (left), CT-Perfusion (middle) and IIF CT-ventilation (right) images for PE case 6 (Table I). For visualization, the intensity values within each image were converted to percentile values (color scale). The red arrows indicate a “wedge” perfusion defect in a region of preserved ventilation on the CT-ventilation image, indicating perfusion/ventilation mismatch that is characteristic of PE.

there is no corresponding wedge defect on the CT-ventilation image, illustrating the potential of CT-P and CT-ventilation to capture this phenomenon on noncontrast CT imaging. However, the current CT-P numerical method smooths the sharp geometric boundaries of the wedge defect. This result is not surprising considering that the MLS parameterization [Eq. (11)] inherently describes a spatially smooth image. Thus, while the Table I correlation results demonstrate proof of principle for the CT-P formulation, additional research is still required to improve the numerical method. Our future work includes exploring different basis functions and numerical approaches, such as finite elements and total variation regularization models that are designed to accommodate spatial discontinuities within the solution image. Moreover, a separate investigation focused on PE diagnosis that involves direct comparison between CT-P, SPECT-P, and CTA would be required to determine the diagnostic utility of CT-P.

This study describes the first mechanistic model designed to compute surrogate perfusion images from noncontrast CT. Though the reported correlations between CT-P and SPECT-P are promising, more research is required to determine the CT acquisition protocol and numerical method implementation that yield the highest physiological fidelity. With further study, the CT-P concept has potential for many clinical applications, including the evaluation of patients with suspected PE. Moreover, generating both perfusion and ventilation information from 4DCT in patients undergoing lung cancer radiotherapy would allow for a complete picture of lung function to be incorporated into functional avoidance radiotherapy. In addition to further imaging validation and optimal implementation studies, our future work will evaluate CT-P in oncologic applications, with particular emphasis on investigating the potential improvements in patient outcomes that might result from integrating CT-Ventilation and CT-perfusion methods into functional avoidance planning.

5. CONCLUSION

In this study, we present the CT-Perfusion numerical method for quantifying pulmonary perfusion from dynamic noncontrast CT imaging. The CT-P formulation computes the magnitude mass changes apparent between inhale and exhale CT images using a series of subregional measurements. The

spatial correlation between CT-P and SPECT-perfusion, as well as its sensitivity to the parameter, τ , which describes the amount of uncertainty associated with the subregional measurements, was assessed in 15 patients with pulmonary embolism and 15 patients with nonsmall cell lung cancer. A parameter sweep revealed that the median CT-P and SPECT-P Spearman correlation was relatively stable with respect to τ in both the PE and lung cancer cohorts. $\tau \in [0.010 \ 0.125]$ yielded the highest overall median Spearman correlation of 0.57. For $\tau = 0.0385$, the median correlation in both cohorts was 0.57, indicating consistent CT-P performance on two imaging datasets acquired for different diseases and on different scanners. Our immediate future work includes determining the CT acquisition protocol and numerical method implementation that yield the highest physiological fidelity for CT-P imaging, as well as exploring potential clinical applications of CT-P.

ACKNOWLEDGMENTS

This work was partially funded through University of Michigan Fast Forward Medical Innovation’s MTRAC for Life Sciences Innovation Hub, a partnership with University of Michigan Tech Transfer and the State of Michigan.

CONFLICT OF INTEREST

The authors have no conflict to disclose.

^{a)}Author to whom correspondence should be addressed. Electronic mail: Edward.Castillo@beaumont.edu.

REFERENCES

- Guerrero T, Sanders K, Noyola-Martinez J, et al. Quantification of regional ventilation from treatment planning CT. *Int J Radiat Oncol Biol Phys.* 2005;62:630–634.
- Castillo R, Castillo E, Martinez J, Guerrero T. Ventilation from four-dimensional computed tomography: density versus Jacobian methods. *Phys Med Biol.* 2010;55:4661.
- Vinogradskiy Y, Rusthoven CG, Schubert L, et al. Interim analysis of a two-institution, prospective clinical trial of 4DCT-ventilation-based functional avoidance radiation therapy. *Int J Radiat Oncol Biol Phys.* 2018;102:1357–1365.

4. Yamamoto T, Kabus S, Bal M, Keall P, Benedict S, Daly M. The first patient treatment of computed tomography ventilation functional image-guided radiotherapy for lung cancer. *Radiother Oncol.* 2016;118:227–231.
5. Yaremko BP, Guerrero TM, Noyola-Martinez J, et al. Reduction of normal lung irradiation in locally advanced non-small-cell lung cancer patients, using ventilation images for functional avoidance. *Intl J Radiat Oncol Biol Phys.* 2007;68:562–571.
6. Wood KE. Major pulmonary embolism: review of a pathophysiologic approach to the golden hour of hemodynamically significant pulmonary embolism. *Chest.* 2002;121:877–905.
7. Hogan S, Greene J, Flemming J. Rate of nondiagnostic computerized tomography pulmonary angiograms (CTPAs) performed for the diagnosis of pulmonary embolism in pregnant and immediately postpartum patients. *Obst Gynecol Internat.* 2019;2019:1432759.
8. Mortensen J, Gutte H. SPECT/CT and pulmonary embolism. *Eur J Nucl Med Mol Imaging.* 2014;41:81–90.
9. Bajc M, Olsson B, Palmer J, Jonson B. Ventilation/perfusion SPECT for diagnostics of pulmonary embolism in clinical practice. *J Intern Med.* 2008;264:379–387.
10. Reinhardt JM, Ding K, Cao K, Christensen GE, Hoffman EA, Bodas SV. Registration-based estimates of local lung tissue expansion compared to xenon CT measures of specific ventilation. *Med Image Anal.* 2008;12:752–763.
11. Castillo E, Castillo R, Vinogradskiy Y, et al. Robust CT ventilation from the integral formulation of the Jacobian. *Med Phys.* 2019;45:2115–2125.
12. Castillo E, Vinogradskiy Y, Castillo R. Robust HU-based CT-ventilation from an integrated mass conservation formulation. *Med Phys.* 2019;46:5036–5046.
13. Simon B. Non-invasive imaging of regional lung function using x-ray computed tomography. *J Clin Monit Comput.* 2000;16:433–442.
14. Guerrero T, Sanders K, Castillo E, et al. Dynamic ventilation imaging from four-dimensional computed tomography. *Phys Med Biol.* 2006;51:777.
15. Jorgenson CC, Coffman KE, Johnson BD. Effects of intrathoracic pressure, inhalation time, and breath hold time on lung diffusing capacity. *Respir Physiol Neurobiol.* 2018;258:69–75.
16. Brecher Gerhard A, Hubay CA. Pulmonary blood flow and venous return during spontaneous respiration. *Circ Res.* 1955;3:210–214.
17. Mahmood SS, Pinsky MR. Heart-lung interactions during mechanical ventilation: the basics. *Ann Translat Med.* 2018;6:349.
18. Cao JJ, Wang YI, Schapiro W, et al. Effects of respiratory cycle and body position on quantitative pulmonary perfusion by MRI. *J Magn Reson Imaging.* 2011;34:225–230.
19. Myziuk N, Guerrero T, Sakthivel G, et al. Pulmonary blood mass dynamics on 4DCT during tidal breathing. *Phys Med Biol.* 2019;64:045014.
20. Castillo R, Castillo E, McCurdy M, et al. Spatial correspondence of 4D CT ventilation and SPECT pulmonary perfusion defects in patients with malignant airway stenosis. *Phys Med Biol.* 2012;57:1855.
21. Ding K, Cao K, Fuld MK, et al. Comparison of image registration based measures of regional lung ventilation from dynamic spiral CT with Xe-CT. *Med Phys.* 2012;39:5084–5098.
22. Castillo E, Castillo R, Vinogradskiy Y, Guerrero T. The numerical stability of transformation-based CT ventilation. *Int J CARS.* 2017;12:569–580.
23. Yamamoto T, Kabus S, Klinder T, et al. Four-dimensional computed tomography pulmonary ventilation images vary with deformable image registration algorithms and metrics. *Med Phys.* 2011;38:1348–1358.
24. Yamamoto T, Kabus S, Lorenz C, et al. 4D CT lung ventilation images are affected by the 4D CT sorting method. *Med Phys.* 2013;40:101907.
25. Yamamoto T, Kabus S, von Berg J, et al. Reproducibility of four-dimensional computed tomography-based lung ventilation imaging. *Acad Radiol.* 2012;19:1554–1565.
26. Fatyga M, Dogan N, Weiss E, et al. A voxel-by-voxel comparison of deformable vector fields obtained by three deformable image registration algorithms applied to 4DCT lung studies. *Front Oncol.* 2015;5:17.
27. Castillo E, Castillo R, Vinogradskiy Y, et al. Technical note: on the spatial correlation between robust CT-ventilation methods and SPECT ventilation. *Med Phys.* 2020;47:5731–5738.
28. Hammersley JM. *Monte Carlo Methods*, 1st edn. Netherlands: Springer; 1964.
29. Cline D, Jeschke S, White K, Razdan A, Wonka P. Dart throwing on surfaces. *Comput Graph Forum.* 2009;28:1217–1226.
30. Delmon V, Rit S, Pinho R, Sarut D. Registration of sliding objects using direction dependent B-splines decomposition. *Phys Med Biol.* 2013;58:1303–1314.
31. Castillo E. Quadratic penalty method for intensity-based deformable image registration and 4DCT lung motion recovery. *Med Phys.* 2019;45:2194–2203.
32. Ruhaak J, Polzin T, Heldmann S, et al. Estimation of large motion in lung CT by integrating regularized keypoint correspondences into dense deformable registration. *IEEE Trans Med Imaging.* 2017;36:1746–1757.
33. Castillo SJ, Castillo R, Castillo E, et al. Evaluation of 4D CT acquisition methods designed to reduce. *J Appl Clin Med Phys.* 2015;16:23–32.
34. Kipritidis J, Tahir BA, Cazoulat G, et al. The VAMPIRE challenge: a multi-institutional validation study of CT ventilation imaging. *Med Phys.* 2019;46:1198–1217.
35. Galbán CJ, Han MK, Boes JL, et al. Computed tomography-based biomarker provides unique signature for diagnosis of COPD phenotypes and disease progression. *Nat Med.* 2012;18:1711–1715.
36. Anderson DR, Kahn SR, Rodger MA, et al. Computed tomographic pulmonary angiography vs ventilation-perfusion lung scanning in patients with suspected pulmonary embolism: a randomized controlled trial. *JAMA.* 2007;298:2743.
37. Moore AJE, Wachsmann J, Chamarthy MR, Panjikaran L, Tanabe Y, Rajiah P. Imaging of acute pulmonary embolism: an update. *Cardiovasc Diagn Ther.* 2017;8:225–243.